Global Change Biology

Global Change Biology (2010) **16**, 3014–3023, doi: 10.1111/j.1365-2486.2010.02164.x

Public Internet-connected cameras used as a cross-continental ground-based plant phenology monitoring system

ERIC A. GRAHAM*, ERIN C. RIORDAN*†, ERIC M. YUEN*, DEBORAH ESTRIN* and PHILIP W. RUNDEL*†

*Center for Embedded Networked Sensing, University of California, Los Angeles, 3563 Boelter Hall, Los Angeles, CA 90095-1596, USA, †Department of Ecology and Evolutionary Biology, University of California, Los Angeles, Los Angeles, CA 90095-1606, USA

Abstract

Plant phenology is highly sensitive to changes in environmental conditions and can vary widely across landscapes. Current observation methods are either manual for small-scale, high precision measurements or by satellite remote sensing for large-scale, low spatial resolution measurement. The development of inexpensive approaches is necessary to advance large scale, high precision phenology monitoring. The use of publicly available, Internet-connected cameras, often associated with airports, national parks, and roadway conditions, for detecting and monitoring plant phenology at a continental scale can augment existing ground and satellite-based methodologies. We collected twice-daily images from over 1100 georeferenced public cameras across North America from February 2008 to 2009. Using a test subset of these cameras, we compared modeled spring 'green-up' with that from co-occurring remote sensing products. Although varying image exposure and color correction introduced noise to camera measurements, we were able to correlate spring green-up across North America with visual validation from images and detect a latitudinal trend. Public cameras had an equivalent or higher ability to detect spring compared with satellite-based data for corresponding locations, with fewer numbers of poor quality days, shorter continuous bad data days, and significantly lower errors of spring estimates. Manual image segmentation into deciduous, evergreen, and understory vegetation allowed detection of spring and fall onset for multiple vegetation types. Additional advantages of a public camera-based monitoring system include frequent image capture (subdaily) and the potential to detect quantitative responses to environmental changes in organisms, species, and communities. Public cameras represent a relatively untapped and freely available resource for supporting large-scale ecological and environmental monitoring.

Keywords: climate change, digital camera, image processing, plant phenology, remote sensing

Received 7 October 2009 and accepted 11 December 2009

Introduction

Plant phenology, the study of the periodic phases of plant development such as budburst, flowering, and leaf senescence, is one of the most responsive and easily observed traits in nature impacted by changing climate (Badeck *et al*., 2004). In the past decade, the advancement of spring onset and the lengthening of the growing season have been detected by both ground (Menzel & Fabian, 1999; Walther *et al*., 2002; van Vliet *et al*., 2003) and satellite observations (Myneni *et al*., 1997; Zhou *et al*., 2001; Slayback *et al*., 2003; Stöckli & Vidale, 2004; Wolfe *et al*., 2005; Cleland *et al*., 2007). Nation-wide observation networks have been founded in both North America and Europe in attempt to document trends in plant growth dynamics at continent-wide scales, as with the U.S. National Phenology Network (USANPN, http://www.usanpn.org; Betancourt *et al*., 2007). Detecting shifts in the timing of plant phenological events, however, is limited by the constraints of existing technologies for observing phenology and difficulties in integrating those technologies (Studer *et al*., 2007; Morisette *et al*., 2009). Development of inexpensive, instrument-based approaches for field measurement is necessary to advance large-scale phenology monitoring (Morisette *et al*., 2009). We present a relatively simple and inexpensive approach for detecting phenological events across North America utilizing public, freely available Internet-connected cameras, often associated with airports, national parks, and roadway conditions, to augment existing satellite and survey-based observations.

Current phenology monitoring methods are either (1) ground-based for small-scale, high precision but labor-intensive measurements or (2) remote sensing-based for

Correspondence: Philip W. Rundel, tel. +1 310 825 8777, fax +1 310 825 9433, e-mail: rundel@biology.ucla.edu

large-scale but low spatial resolution measurements, often too coarse to detect species and community level responses (Badeck *et al*., 2004). Ground-based vegetation monitoring allows precise measurements of phenology, but only over a restricted area, number of individuals, or species because of high labor cost. The use of ground-based measurements for the validation of remote sensing data is difficult (see Studer *et al*., 2007) because phenological events are usually unevenly distributed and the quality of ground-based data is often dependent on a qualitative observer (Menzel, 2002) or is based on variable local data collection methods (Cleland *et al*., 2007). Nevertheless, strategically linking satellite-based sensing of broad regions with finer-scale, on-the-ground monitoring is vital for improving early detection of ecologically significant changes in phenology (Hargrove *et al*., 2009).

While satellite technology enables the detection of continuous landscape to global vegetation dynamics at low cost to scientists, attempts to track changes in phenology during climate change from these products have only been moderately successful (Schwartz, 1990; Kathuroju *et al*., 2007). Satellite-based indices of surface reflectance, such as the normalized difference vegetation index (NDVI), provide a measure of vegetation 'greenness' (Reed *et al*., 1994; Myneni *et al*., 1995, 1997; Zhou *et al*., 2001; Pettorelli *et al*., 2005). However, noise in these signals (Reed *et al*., 1994; Cihlar *et al*., 1997; Huete *et al*., 2002; Thayn & Price, 2008; Hird & McDermid, 2009) can make detection of fine scale temporal changes difficult. Challenges in using satellite data are due in part to its sensitivity to effects of clouds and atmospheric conditions, but also the lack of parallel ground-based phenological observations (Fisher & Mustard, 2007) and scalable field models (Fisher *et al*., 2007). Furthermore, the individual pixels in a remotely sensed image can include unknown combinations of species, forest types, and land use types, making it nearly impossible to detect critical organism, species, or community-level responses (Fisher *et al*., 2006). Although methods for scaling up ground-based measurements are still lacking, new advancements in field monitoring technologies, such as the use of visible light digital cameras, hold promise (Richardson *et al*., 2007; Crimmins & Crimmins, 2008; Graham *et al*., 2009; Morisette *et al*., 2009).

The use of visible-light digital cameras in ecological applications has increased dramatically in recent years, including both hand-held high-resolution and fixed location lower-resolution video cameras mounted in public locations. Most of this increase in use has been due to the reduction in cost, size, and the increase in the data communication abilities of digital cameras. Thus, visible-light digital cameras are becoming common place in research for quantitatively describing vegetation growth and biomass (Boyd & Svejcar, 2005; Crimmins & Crimmins, 2008; Graham *et al*., 2009), nitrogen status and plant stresses (Wang *et al*., 2004), and within-canopy green-up and senescence (Fisher *et al*., 2006). Indeed, simple image processing techniques are making standard the use of digital cameras for the detection of phenological events (Richardson *et al*., 2007; Graham *et al*., 2009; Morisette *et al*., 2009) as well as for automating a range of agricultural monitoring practices (Slaughter *et al*., 2008).

The digital images from publicly accessible, Internet-connected cameras established for nonscientific monitoring applications represent a relatively untapped, inexpensive, and easily acquired resource for augmenting large scale phenology monitoring. We propose the use of the thousands of freely available public cameras associated with monitoring natural areas, roadway conditions, and for human surveillance as a novel means for detecting and monitoring plant phenology at a continental scale. Our methodologies for detecting changes in vegetation greenness are simple and similar to those used in previous phenology studies using digital images and the model we use to detect the timing of spring green-up and fall senescence events is a common approach used in satellite-based methods. We compare our detection with that of freely available satellite remote sensing Moderate Resolution Imaging Spectroradiometer (MODIS) products used for large-scale environmental monitoring.

Materials and methods

Public camera acquisition and image processing

Using key word searches on a popular Internet search engine (Google), we manually identified over 1400 publicly available cameras for capturing images with vegetation across North America during 1 week starting February 1, 2008. Public camera physical locations were initially determined from their Internet protocol (IP) addresses. Images were automatically captured twice daily, once at 10:00 and once at 15:00 hours, local camera time, and stored in a local database (MySQL; Sun Microsystems Inc., Santa Clara, CA, USA). Of these, a subset of 30 public cameras was chosen as a test group to represent a range of habitats and locations across North America based on camera performance (stationary point of view, and few malfunctions or missing images). Additionally, each location of the subset of public cameras was then manually revised to a more accurate latitude and longitude (datum WGS84) using information included on the supporting web page that hosted the public camera image (Fig. 1, Table 1).

After each image was collected, a value was calculated for whether the images was too dark or too light based on the grey-scale pixel average and the average excess green ($2 \times$ value of the green pixel$-$value of the red pixel$-$value of

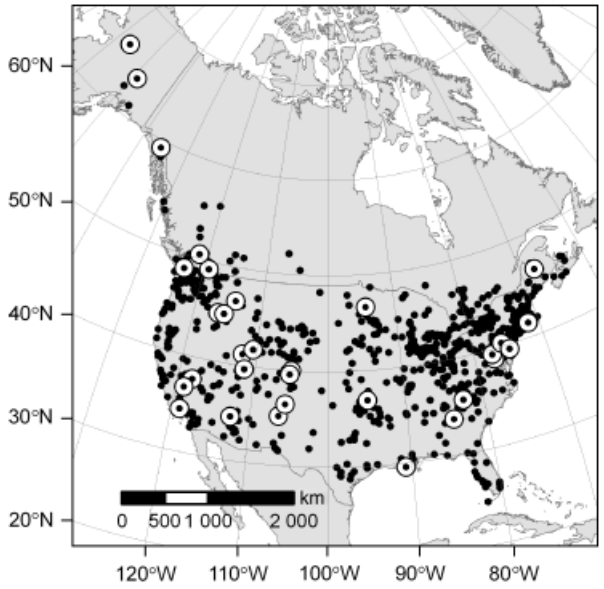

Fig. 1 Locations of the 1141 Internet-accessible public cameras identified in the winter of 2008 as containing vegetation for phenology monitoring. Bull's-eye points indicate the subset of 30 test locations.

the blue pixel; Woebbecke *et al*., 1995; Meyer & Neto, 2008). Both values were stored with the image metadata in the database. For each test public camera, a mask was manually created to separate deciduous, evergreen, and understory vegetation from nonvegetated areas in the image. For these images, the excess green values in the areas of interest were also averaged.

Additionally, we visually inspected the time series of images from each test public camera and manually recorded the date at which the deciduous vegetation began to show green in the spring (10% green), was fully green in the summer (90% green), and the first signs of leaf senescence in the fall (10% nongreen leaf color), establishing a visual ground truth to the test public camera data set.

Satellite imagery acquisition and processing

To evaluate our detection of vegetation dynamics from public camera images, we obtained satellite imagery for the same geographic locations as those of the test public camera locations. Daily MODIS images of surface reflectance (MOD09GA) at 500 m resolution were obtained from January 1 to December 31, 2008 for the extent of North America containing public camera locations. A satellite-based land cover classification (MCD12Q1) for the location of each public camera was also obtained for the most recent year available, 2005. This land cover classification was used as a further validation that public camera images and MODIS reflectance data were considering similar vegetation types. Land cover and daily surface reflectance products were downloaded from the Warehouse Inventory Search Tool (https://wist.echo.nasa.gov/wist/api/imswelcome). We identified the tile, scan, and line for each public camera geolocation in the native MODIS sinusoidal projection using the University of Oklahoma's Earth Observation and Modeling group's data visualization tool (http://www.eomf.ou.edu/). The NDVI was calculated from the red (RED 620–670 nm) and near infrared (NIR 841–876 nm) bands of the surface reflectance product as: (NIR−RED)/(NIR + RED). We used per pixel quality assurance scientific data sets to identify and remove poor quality surface reflectance data.

For each of the public cameras in our test subset, we located the corresponding remote sensing pixel and surrounding eight pixels to form a 3×3 pixel matrix. Any pixels flagged as containing the maximum value of clouds, high atmospheric or cirrus effects, or general low quality, were removed from our analyses. For each point in time, the median of the remaining high-quality pixels in the daily 3×3 pixel matrix was calculated to create a final cleaned satellite NDVI time series for the central, corresponding location of the public camera.

Detection of phenological events

Both public camera excess green and satellite NDVI time series for 2008 were modeled using an asymmetric double sigmoid function (Soudani *et al*., 2008) based on the logistic equations of Fisher *et al*. (2006) and Zhang *et al*. (2003).

$$\text{NDVI \& excess green} = (w_1 + w_2) + 0.5 \times (w_1 - w_2) \times [\tanh(w_3 \times (t - u)) - \tanh(w_4 \times (t - v))],$$

where tanh is the hyperbolic tangent, t is the time (Julian day), $(w_1 + w_2)$ the greenness minimum, $(w_1 - w_2)$ the total amplitude of the greenness signal, and u and v are the dates corresponding to the highest rates of change of the fitted greenness function. The parameters u and v can thus be used directly as estimates of spring leaf expansion, or fall leaf senescence (Soudani *et al*., 2008). We used a nonlinear least squares regression method in the STATS statistical package in the freely available statistical analysis program R (version 2.9.0, *R* Development Core Team, http://www.R-project.org) to model NDVI and excess green time series and estimate fitting parameters. Initial parameter estimates were calculated from a local polynomial regression fitting (loess) smooth of the data.

For each public camera excess green and satellite time series, we also applied a five-point moving mean $\pm 20\%$ window to remove outlying points and further smooth the data and facilitate model fitting. Because we were able to capture multiple images from public cameras per day, we chose the model fits with lowest standard errors for estimates of spring to compare with satellite data. Statistical comparison between public cameras and satellite pixels were conducted for locations where only one maximum occurred for the loess smooth of the data and the standard error of the estimate of spring was <16 days, equivalent to the MODIS 16 days product commonly used for analysis of dates of onset of spring.

Table 1 Locations and descriptions of the 30 public camera test subset (hand segmentation categories abbreviated as following: deciduous vegetation indicated by dec, evergreen as ever, and understory grass as grass)

Public camera	Latitude	Longitude	US State	Elevation (m)	Segmentation category	Visual camera classification	Satellite classification
872	59.22	−135.43	AK	56	Dec, ever	Mixed forest	Mixed forest
878	65.70	−156.35	AK	57	Ever, grass	Evergreen, understory annuals	Evergreen Needle-leaf forest
904	63.73	−148.91	AK	503	Dec, ever	Mixed forest	Evergreen Needle-leaf forest
970	34.40	−118.92	CA	171	Dec, ever	Open shrublands	Open shrublands
994	37.68	−118.08	NV	1494	Dec, ever	Open shrublands	Open shrublands
1014	34.56	−112.45	AZ	1646	Dec	Urban	Urban and built-up
1051	36.72	118.96	CA	1946	Ever	Evergreen forest	Evergreen Needle-leaf forest
1146	46.51	−114.09	MT	1036	Dec, ever, grass	Evergreen, deciduous, urban	Grasslands
1331	48.61	−123.15	WA	30	Ever, grass	Evergreen and pasture	Evergreen Needle-leaf forest
1350	39.63	−111.44	UT	1839	Dec, ever, grass	Open shrublands	Open shrublands
1433	49.15	−119.24	BC	1941	Ever, grass	Evergreen and grass – ski resort	Evergreen Needle-leaf forest
1444	50.42	−121.35	BC	472	Dec, ever, grass	Evergreen, deciduous, urban	Savannas
1447	35.17	−106.36	NM	2133	Ever, grass	Evergreen and pasture – golf course	Grasslands
1451	36.44	−105.58	NM	2145	Dec, grass	Grasslands	Grasslands
1473	39.95	−105.02	CO	1615	Grass	Urban, soccer field	Urban and built-up
1511	36.89	−94.88	OK	234	Dec, grass	Urban and built-up	Urban and built-up
1542	29.57	−90.74	LA	1	Dec, grass	Urban and built-up park	Croplands
1584	46.60	−94.31	MN	390	Dec, grass	Deciduous and grassland	Cropland/Natural vegetation mosaic
1605	33.80	−84.17	GA	309	Ever	Urban and built-up	Urban and built-up
1622	35.58	−82.55	NC	658	Dec	Shrubland, riparian, urban	Urban and built-up
1698	38.95	−77.34	VA	114	Dec, grass	Deciduous, urban	Urban and built-up
1859	39.44	−77.54	MD	179	Dec, grass	Croplands, fallow grass	Croplands
1891	40.04	−75.49	PA	143	Dec, grass	Urban and built-up park	Urban and built-up
1923	40.34	−75.93	PA	76	Dec	Urban and built-up park	Urban and built-up
2007	41.44	−71.50	RI	17	Dec	Urban and built-up park	Mixed forest
2065	39.49	−75.03	NJ	30	Dec, grass	Urban and built-up grass	Urban and built-up
2077	44.96	−116.39	ID	1283	Ever	Evergreen Needle-leaf forest	Evergreen Needle-leaf forest
2088	44.97	−115.49	ID	1521	Ever, grass	Grassland, Evergreen	Evergreen Needle-leaf forest
2251	39.57	−105.22	CO	2202	Dec, ever, grass	Rural mixed forest	Evergreen Needle-leaf forest
2269	46.31	−67.84	ME	126	Dec, ever, grass	Cropland/Natural vegetation mosaic	Cropland/Natural vegetation mosaic

Results

Of our initial 1495 public cameras, we were able to georeference 1141 public cameras (Fig. 1). During our study, public cameras were lost, through cameras going offline or through changes in their IP addresses, at a steady rate of 0.442 per day ($r^2 = 0.998$). A subset of all public cameras were also moved during our sampling, either by users of the camera or by their owners, further reducing the number of immediately useful public cameras.

Both public camera and satellite pixel green-up signals had high day to day and between location variability (Fig. 2). Image over- and under-exposure and automatic white balance introduced noise to public camera excess green measurements of vegetation (Fig. 2b and d), while cloud cover and varying atmospheric conditions introduced noise to satellite NDVI time series (Fig. 2a and c). Overall, the test group of public cameras had fewer days flagged as poor quality ($P < 0.0001$; Wilcoxon's signed-rank test) and shorter gaps of consecutive bad days ($P = 0.0001$; Wilcoxon's signed-rank test) compared with the corresponding satellite data series for the same locations (Table 2). The median total number of poor quality days for public camera excess green time series was 14 (range: 0–59) compared with 173 (range: 66–238) for satellite NDVI time series. Similarly, the median gap of consecutive poor quality days was 2 (range: 0–13) for public camera series compared with 10 (range: 5–25) for satellite series.

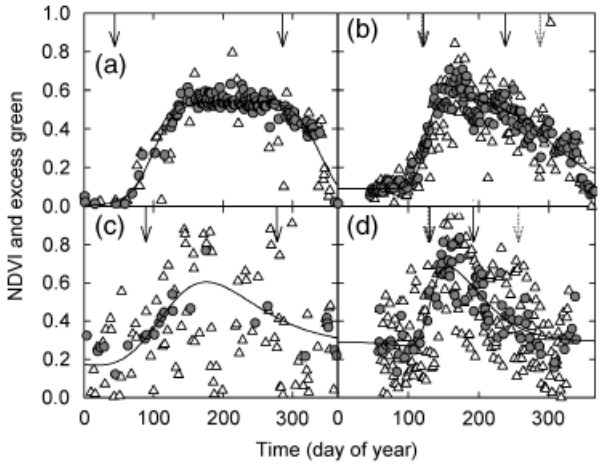

Fig. 2 Satellite (a, c; NDVI) and public camera (b, d; excess green) greenness signals at two test locations (location #1331 for a and b; #872 for c and d) during 2008. Daily data (open triangles) exclude poor quality data points (i.e., satellite images collected under the highest cloud cover and over and under-exposed public camera images). Filled circles are cleaned daily data that lie within ±20% of the mean of the two previous and two sequential daily data. A double sigmoid model was fitted to the daily data. Solid arrows indicate the modeled spring and fall dates and dashed arrows indicate visual estimate of the day at which public camera images contained 10% greenness for spring and 10% fall colors.

From the 922 public cameras that were successfully modeled using whole-image excess green, the mean date of spring occurred at 110.7 ± 38.7 days. The maximum date of estimated spring occurred at 234.4 days and a minimum at 46.0 days. For the subset of 30 public camera test locations, the mean date of spring occurred at 110.0 ± 33.0 days, the maximum at 191 days and the minimum at 25 days. Dates of spring and fall were also estimated for our subset of public cameras from visual inspection of image sequences. The mean date of visual spring occurred at 109.8 ± 22.1 days, the maximum at 151 days and a minimum at 56.0 days. We illustrate these estimates with two examples, one at a location having relatively 'clean' green series for both public camera and satellite imagery (location #1331, Fig. 2a and b), and one at a location having noisy green series for both public camera and satellite imagery (location #872, Fig. 2c and d). For the clean time series, public camera and satellite models had similar performance in terms of error associated with the spring estimate. The modeled day of spring for location #1331 for the satellite was 100.1 ± 3.8 days (estimate ± standard error; Fig. 2a) and 118.9 ± 2.9 days for the public camera (Fig. 2b); the visual estimation of spring (50% green) for the public camera occurred on day 117. In contrast, for the noisy time series, public camera data yielded models with much lower error associated with spring estimate than satellite data. The modeled day of spring for location #872 for the satellite was 95.6 ± 12.3 days (Fig. 2c) and 138.6 ± 3.3 days for the public camera (Fig. 2d); the visual estimation of spring for the public camera occurred on day 132.

Public camera excess green series had better double sigmoid model fits, in terms of RMSE, compared with corresponding satellite NDVI series (one-tailed Wilcoxon's signed-rank test, $P = 0.02$), however, this difference was not significant after the 20% mean filter was applied to both data sets (one-tailed Wilcoxon's signed-rank test, $P = 0.06$; Table 2). Additionally, the estimated spring dates from total image excess green had significantly lower errors than corresponding satellite NDVI estimates (Table 2). Application of the 20% mean filter to cleaned data sets improved model RMSE in all cases (all $P < 0.001$), however, this only resulted in an improvement of the spring estimate standard error in the satellite NDVI (one-tailed Wilcoxon's signed-rank test, $P = 0.015$; all other $P > 0.18$).

Hand-segmentation of our 30 public camera test locations yielded 21 deciduous, 16 evergreen, and 21 understory excess green time series. We were able to

Table 2 Model performance, root mean squared error (RMSE), and standard error (SE) of the spring estimate, reported as median and range (min–max)

	All ExG	Deciduous	Evergreen	Understory	Satellite
RMSE	0.1224*	0.0965**	0.1362	0.1441	0.1457
	(0.0786–0.1987)	(0.0712–0.1567)	(0.0919–0.2014)	(0.0812–0.1790)	(0.0940–0.1993)
	($n = 25$)	($n = 20$)	($n = 12$)	($n = 15$)	($n = 21$)
RMSE 20% filter	0.0793	0.0816**	0.0754	0.0998	0.0977
	(0.0323–0.1669)	(0.0461–0.1141)	(0.0539–0.1226)	(0.0505–0.1529)	(0.0713–0.1495)
	($n = 28$)	($n = 20$)	($n = 14$)	($n = 18$)	($n = 20$)
Spring SE	1.7411**	0.8854***	2.9193	1.6833**	5.0745
	(0.5230–10.7939	(0.4152–2.6344)	(0.2286–9.3014)	(0.6432–7.6180)	(1.1425–15.5337)
	($n = 25$)	($n = 20$)	($n = 12$)	($n = 15$)	($n = 21$)
Spring SE 20% filter	1.6849**	0.8377**	2.7624*	1.8278**	3.6952
	(0.5622–9.4710)	(0.4730–15.3050)	(0.5864–9.9194)	(0.7318–6.4100)	(0.5230–10.7940)
	($n = 28$)	($n = 20$)	($n = 14$)	($n = 18$)	($n = 20$)

*Significance at $P < 0.05$; **$P < 0.01$; ***$P < 0.001$ for one-tailed Wilcoxon's signed-rank tests comparing public camera models with satellite models.

successfully model excess green values for all but two public camera locations after the application of the 20% mean filter, and failed for one deciduous, two evergreen, and three understory subset public camera time series. In contrast, we were unable to model nine of the corresponding satellite NDVI time series, even with the application of the 20% mean filter. Image segmentation led to a significant improvement in deciduous spring estimates (one-tailed Wilcoxon's signed-rank test, $P = 0.02$), but there was no corresponding improvement in evergreen or understory data. Model RMSE was comparable for all segmented vegetation types (Kruskal–Wallis test, $P = 0.17$, df = 3). Overall, public camera models had slightly lower RMSE than satellite models, though this was only significant for the deciduous subset. Public camera models had significantly lower error associated with spring estimates compared with satellite models (all $P < 0.05$, Table 2).

As an example, for a representative subset of these hand-segmented locations from the public cameras (Fig. 3), the lowest RMSE for the model for deciduous data was 0.083 (Fig. 3e) and the estimate for the date of spring ranged from April 29 ± 2.7 days (estimate ± standard error; Fig. 3i) to June 5 ± 0.7 days (Fig. 3e). Dates of the estimates for spring varied between the deciduous (Fig. 3a, e, i, and m), evergreen (Fig. 3b, f, j, and n), and understory (Fig. 3c, g, k, and o) components. The maximum difference within one location of 54.5 days occurred between the evergreen (June 5 ± 7.3 days; Fig. 3j) and understory (April 10 ± 2.1 days; Fig. 3k) components, and the minimum of 5.7 days within a location occurred between the deciduous (June 5 ± 0.7 days; Fig. 3e) and evergreen (May 30 ± 1.4 days; Fig. 3f) components.

Public camera modeled spring estimates for deciduous vegetation most closely correlated with the 50% green visual ground truths ($r = 0.98$; Pearson's correlation coefficient; Fig. 4a), and the beginning of spring 10% green ($r = 0.977$), and the summer 90% green values ($r = 0.96$) were also closely correlated. The 20% filtered data had only a slightly lower correlation with all 10%, 50%, and 90% ground truth dates ($r \geqslant 0.94$). The mean difference between 50% green visual ground truth and modeled estimates for deciduous vegetation was 0.09 ± 7.87 days (mean ± SD). Visual estimates of 50% spring for understory vegetation (Fig. 4c) was also correlated with model estimates ($r = 0.72$) and the mean difference between the two was 10.2 ± 12.6 days. Visual estimates of spring for evergreen vegetation were not correlated with modeled values ($r = 0.05$). Validating satellite-based estimates requires intensive ground truthing, which were not available for our data set.

Visual estimates of fall, defined as 10% nongreen leaf color from public camera images, were less well correlated with modeled data than spring estimates for both deciduous ($r = 0.75$; Fig. 4b) and understory ($r = 0.69$; Fig. 5d) vegetation. Mean differences were relatively large for deciduous vegetation (31.9 ± 41.1 days) and less so for understory vegetation, although the variance was similarly high (2.1 ± 35.0 days).

We observed a latitudinal trend in the test public camera set of estimated ($r^2 = 0.44$) and visual (50% green; $r^2 = 0.40$) dates of spring for deciduous vegetation (Fig. 5a), but none in the estimated dates of fall ($r^2 < 0.006$ for both; Fig. 5b). There was no discernable latitudinal trend from satellite data for either spring or fall onset ($r^2 < 0.004$; Fig. 5c and d) for this subset of locations. Including an interaction of elevation with

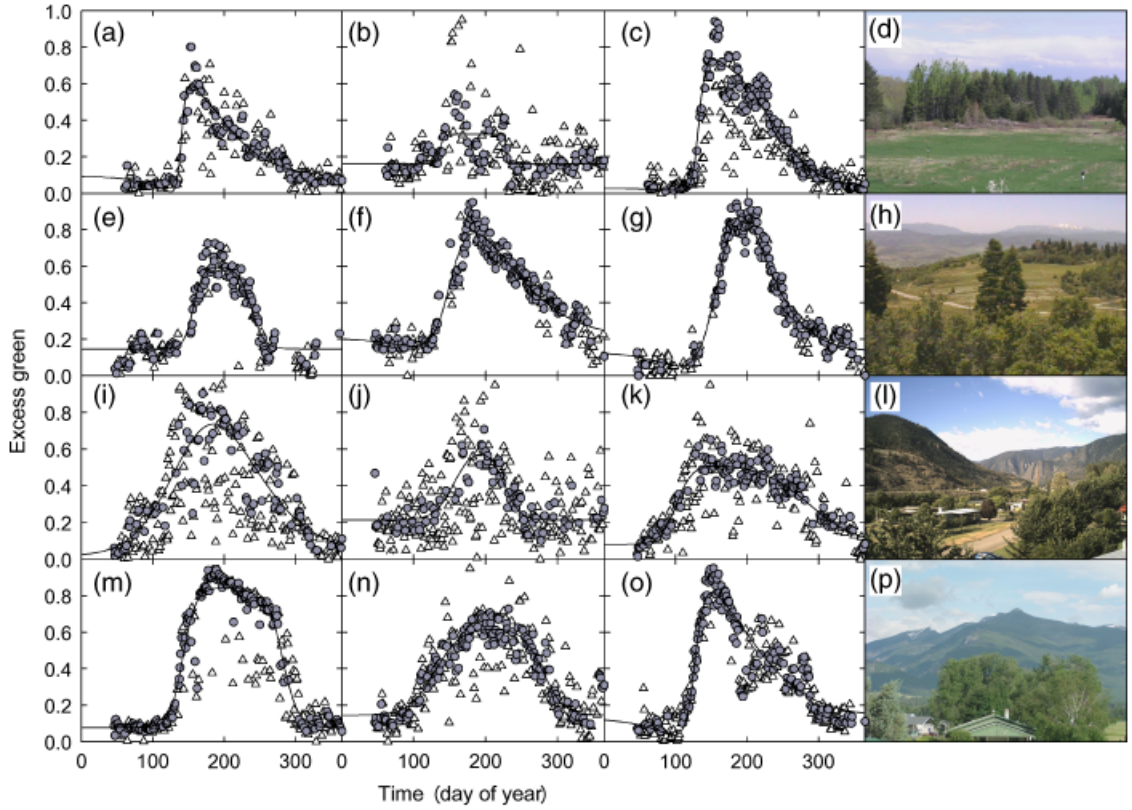

Fig. 3 Greenness signals for hand-segmented deciduous (a, e, i, m), evergreen (b, f, j, n), and understory (c, g, k, o) regions within images at four test public camera (location #2269 for row a, #1350 for row e, #1444 for row i, and #1146 for row m) containing all three vegetation types during 2008. Example images from late June 2008 are included (d, h, l, p). Symbols and curves as in previous figure.

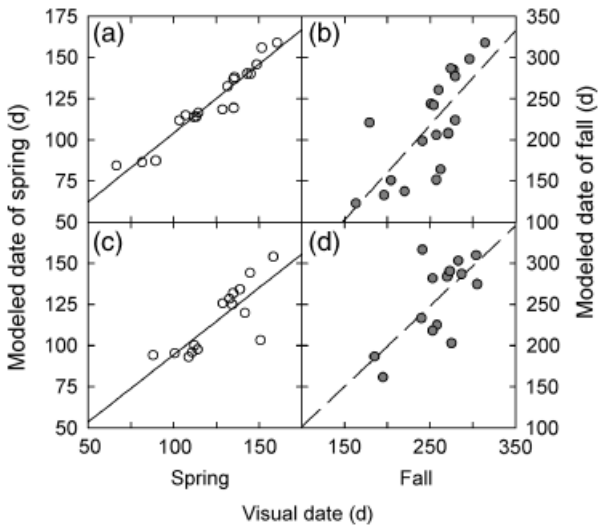

Fig. 4 Visually established date of spring (open symbols) and fall (filled symbols) compared with modeled estimates of spring and fall for deciduous (a and b) and understory (c and d) vegetation. Date of visual spring is based on 50% green and date of modeled spring is based on the first inflection point of the double sigmoid model. Date of visual fall is based on 10% fall colors and the date of modeled fall is the second inflection point.

latitude also did not result in a statistically significant correlation with the onset of spring or fall and latitude for the satellite data ($r^2 < 0.15$).

Discussion

Public Internet-connected cameras represent a relatively untapped, easily accessible, and highly valuable resource for large-scale ecological observation, complementing current ground- and satellite-based systems for monitoring global climate change. While recent studies have used high resolution, networked digital cameras to provide a near surface remote sensing of phenological events at specific study locations (Richardson *et al*., 2007, 2009; Ahrends *et al*., 2008; Crimmins & Crimmins, 2008), we demonstrate the use of thousands of publicly available cameras associated with airports, national parks, and roadway conditions coupled with simple image processing to detect phenological events at a continental scale.

Our predictions of the timing of spring were most reliable for deciduous and understory vegetation, with a high correlation to visual 'ground truths' in our subset

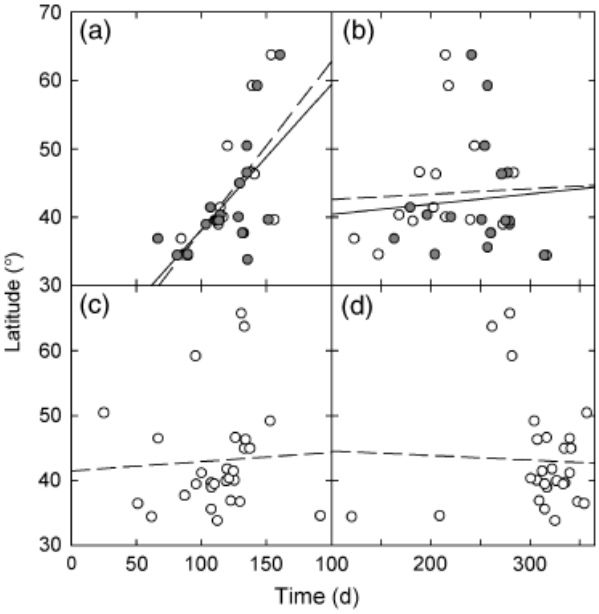

Fig. 5 Latitudinal trends in the estimated dates (open circles; dashed lines) of spring (a and c) and fall (b and d) deciduous vegetation from public cameras (a and b) and corresponding satellite pixels (c and d). Spring and fall onset dates determined by visual inspection (10% spring or fall color) are included in public camera regressions (filled circles; solid lines).

of 30 cameras. We were able to detect the date of spring in these camera images with greater confidence than in satellite images (because of both a smaller SE and the availability of a visual ground truth), however, there was no statistically significant difference between the dates themselves derived from the two methods. Because we used the point of inflection of the double sigmoid model to estimate the date of spring rather than the initial appearance of green leaves in images, this was not surprising. While we predicted a spring green-up date for evergreen vegetation, we were unable to correlate this with a visual ground truth in any of our test public cameras, as there was no clear visible flushing of evergreen needles or leaves in these image sequences. Surrounding deciduous vegetation may have affected the color balance of the entire image, including evergreen foliage, contributing to a spring signal. Alternatively, biochemical changes in the composition of existing evergreen foliage may have also resulted in changes in foliage color that were not correlated with the visual occurrence of new leaves (Richardson *et al*., 2009).

Predicting fall senescence dates from satellite data has proved to be less reliable than predicting spring onset dates (Reed *et al*., 1994; Delbart *et al*., 2005). Fall estimates from our test public cameras using excess green were positively correlated with visual ground truths, although not as well as for spring, similar to satellite data. However, the RGB color channels of digital photographs allow for additional (e.g., red-based) indices for detecting changes in vegetation. Although these alternative methods were not tested in this study, such methods show promise for more accurately calculating timing of fall senescence (Richardson *et al*., 2009).

Although measuring at a different spatial scale, we show that public cameras have significantly higher data quality, in terms of data gaps and number of poor quality images, compared with satellite imagery. Indeed, we detected a latitudinal trend in the timing of spring for deciduous vegetation across North America for our test subset of 30 public camera locations that was not evident in the satellite data. This is likely due to public cameras' lower sensitivity to cloud cover which completely masks green-up signals in satellite imagery, although clouds can alter illumination in images and affect automatic color balance in digital cameras. In addition, the significantly lower standard errors associated with spring estimates from public camera time series, compared with those of MODIS imagery, indicate a greater sensitivity to fine-scale temporal difference in the timing of phenological events. Cloud cover, atmospheric effects, aerosols, and effects of viewing angle all introduce noise into satellite-based greenness signals detected from vegetation that increase error in model estimates of phenological signals (Holben, 1986; Reed *et al*., 1994; Huete *et al*., 2002; Vermote *et al*., 2002; Hird & McDermid, 2009). MODIS provides a composited vegetation index product at 16-day intervals that has much fewer cloud effects, however errors associated with these temporally degraded data sets are approximately $\pm$ 10 days, too coarse for detecting shifts in timing of phenological events (Thayn & Price, 2008).

Linking satellite-detected vegetation dynamics to ground processes has proven to be difficult, often because a single pixel (approximately 500 m^2 in this study) within a satellite image can often contain a number of vegetation or land cover types. Dominant vegetation may mask the dynamics of understory or less prevalent species of interest (Badeck *et al*., 2004). Public cameras, however, offer an additional level of detail that is unavailable in satellite imagery without exhaustive ground truthing. Indeed, a pioneer study using ground-based camera images compared with remote sensing data demonstrated that small-scale topography resulted in complex local variation in phenology (Fisher *et al*., 2006), highlighting the need to incorporate local processes when scaling to regional representations. The interpretation of captured public camera images is also possible both by human and

computer vision techniques. Thus, the segmentation of digital images into areas of interest corresponding to vegetation type, such as the deciduous, understory, or even species or individuals, enables the detection of more precise phenological events at small spatial scales. However, the proliferation of Internet-connected public cameras is creating a situation where the global image data stream will soon require unsupervised methods for image analysis and data reduction.

Problems specific to public camera-based phenological monitoring include widely varying image resolution among the public cameras we identified. Cameras intended for air quality monitoring, for example, had very high resolution (1024×768 or higher), while those intended for traffic monitoring tended to have low resolution (640×480 or lower). Additionally, lack of control over public camera operation resulted in changed Internet addresses, removed cameras, and changes in view angle without warning. As in other studies using digital camera-based greenness detection, automatic white/color balance added variability to greenness time series unrelated to changes in vegetation (e.g., Panneton & Brouillard, 2009).

Despite these challenges, Internet-connected public cameras can contribute greatly to phenological monitoring and our ability to detect changes in our environment. While public cameras are no substitute for the continuous measures of vegetation dynamics at large, global scales gained from satellite imagery, they can provide useful information about phenological events at locations spanning regional to global scales. Public cameras can also augment ground-based phenological monitoring which provides the exact timing of budburst for individual plants, but at considerable labor cost and often limited to small areas. Public cameras provide inexpensive, easily accessible, and high frequency monitoring (minute to daily image capture) at a wide number of locations, covering a much larger area than possible with traditional ground monitoring. Furthermore, active research in color detection, computer vision, and cyber infrastructure promises to streamline and automate digital camera-based monitoring in the future, further reducing human costs of field detection.

We have demonstrated that large-scale and high-resolution phenology monitoring can be accomplished using freely available resources, specifically Internet-connected public cameras, simple image processing, and straight-forward phenology models using open-source programming and data analysis software (PYTHON, R). Websites providing access to archived images, such as that being developed (Bradley *et al.*, 2010), will make both imagery and basic image analyses even more easily accessible. We foresee that public camera imagery will soon prove to be an important resource in scaling between ground and satellite for the detection of plant phenological events and monitoring global climate change (Hamilton *et al.*, 2007).

Acknowledgements

The authors wish to thank Eric Howard and Eric Wang for contributing to data analysis. This research was supported by National Science Foundation award 0120778 to the Center for Embedded Networked Sensing at the University of California, Los Angeles.

Authorship: E.A.G. and E.C.R. were equally responsible for designing and performing the research, analyzing data, and writing the paper; E.M.Y. was responsible for performing the research, analyzing data, and contributing analytic tools; D.E. and P.W.R. were responsible for providing scientific leadership and collaboratively writing the paper.

References

Ahrends HE, Brügger R, Stöckli R *et al.* (2008) Quantitative phenological observations of a mixed beech forest in northern Switzerland with digital photography. *Journal of Geophysical Research*, **113**, G04004, doi: 10.1029/2007JG000650.

Badeck F-W, Bondeau A, Böttcher K, Doktor D, Lucht W, Schaber J, Sitch S (2004) Responses of spring phenology to climate change. *New Phytologist*, **162**, 295–309.

Betancourt JL, Schwartz MD, Breshears DD *et al.* (2007) Evolving plans for the USA National Phenology Network – National Phenology Network 2nd Implementation Workshop, Milwaukee, WI, 10–12 October 2006. EOS Transactions, American Geophysical Union, **88**, 211.

Boyd CS, Svejcar TJ (2005) A visual obstruction technique for photo monitoring of willow clumps. *Rangeland Ecology and Management*, **58**, 434–438.

Bradley E, Roberts D, Still C (2010) Design of an image analysis website for phenological and meteorological monitoring. *Environmental Modelling & Software*, **25**, 107–116.

Cihlar J, Ly H, Li ZQ, Pokrant H, Huang FT (1997) Multitemporal, multichannel AVHRR data sets for land biosphere studies–artifacts and corrections. *Remote Sensing of Environment*, **60**, 35–57.

Cleland EE, Chuine I, Menzel A, Mooney HA, Schwartz MD (2007) Shifting plant phenology in response to global change. *Trends in Ecology and Evolution*, **22**, 357–365.

Crimmins MA, Crimmins TM (2008) Monitoring plant phenology using digital repeat photography. *Environmental management*, **41**, 949–958.

Delbart N, Kergoat L, Le Toan T, Lhermitte J, Picard G (2005) Determination of phenological dates in boreal regions using normalized difference water index. *Remote Sensing of Environment*, **97**, 26–38.

Fisher JI, Mustard JF (2007) Cross-scalar satellite phenology from ground, Landsat, and MODIS data. *Remote Sensing of Environment*, **109**, 261–273.

Fisher JI, Mustard JF, Vadeboncoeur MA (2006) Green leaf phenology at landsat resolution: scaling from the field to the satellite. *Remote Sensing of the Environment*, **100**, 265–279.

Fisher JI, Richardson AD, Mustard JF (2007) Phenology model from surface meteorology does not capture satellite-based greenup estimations. *Global Change Biology*, **13**, 707–721.

Graham EA, Yuen EM, Robertson GF, Kaiser WJ, Hamilton MP, Rundel PW (2009) Budburst and leaf area expansion measured with a novel mobile camera system and simple color thresholding. *Environmental and Experimental Botany*, **65**, 238–244.

Hamilton MP, Graham EA, Rundel PW, Allen MF, Kaiser W, Hansen MH, Estrin DL (2007) New approaches in embedded networked sensing for terrestrial ecological observatories. *Environmental Engineering Science*, **24**, 192–204.

Hargrove WW, Spruce JP, Gasser GE, Hoffman FM (2009) Toward a national early warning system for forest disturbances using remotely sensed canopy phenology. *Photogrammetric Engineering and Remote Sensing*, **75**, 1150–1156.

Hird JN, McDermid GJ (2009) Noise reduction of NDVI time series: an empirical comparison of selected techniques. *Remote Sensing of Environment*, **113**, 248–258.

Holben BN (1986) Characteristics of maximum-value composite images from temporal AVHRR data. *International Journal of Remote Sensing*, **7**, 1417–1434.

Huete A, Didan K, Miura T, Rodriquez EP, Gao X, Ferreira LG (2002) Overview of the radiometric and biophysical performance of the MODIS vegetation indices. *Remote Sensing of Environment*, **83**, 195–213.

Kathuroju N, White MA, Symanzik J, Schwartz MD, Powell JA, Nemani RR (2007) On the use of the advanced very high resolution radiometer for development of prognostic land surface phenology models. *Ecological Modelling*, **201**, 144–156.

Menzel A (2002) Phenology: its importance to the global change community – an editorial comment. *Climatic Change*, **54**, 379–385.

Menzel A, Fabian P (1999) Growing season extended in Europe. *Nature*, **397**, 659–659.

Meyer GE, Neto JC (2008) Verification of color vegetation indices for automated crop imaging applications. *Computers and Electronics in Agriculture*, **63**, 282–293.

Morisette JT, Richardson AD, Knapp AK *et al*. (2009) Tracking the rhythm of the seasons in the face of global change: phenological research in the 21st century. *Frontiers in Ecology and the Environment*, **7**, 253–260.

Myneni RB, Hall FG, Sellers PJ, Marshak AL (1995) The interpretation of spectral vegetation indexes. *IEEE Transactions on Geoscience and Remote Sensing*, **33**, 481–486.

Myneni RB, Keeling CD, Tucker CJ, Asrar G, Nemani RR (1997) Increased plant growth in the northern high latitudes from 1981 to 1991. *Nature*, **386**, 698–702.

Panneton B, Brouillard M (2009) Colour representation methods for segmentation of vegetation in photographs. *Biosystems Engineering*, **102**, 365–378.

Pettorelli N, Vik JO, Mysterud A, Gaillard JM, Tucker CJ, Stenseth NC (2005) Using the satellite-derived NDVI to assess ecological responses to environmental change. *Trends in Ecology & Evolution*, **20**, 503–510.

Reed BC, Brown JF, Vanderzee D, Loveland TR, Merchant JW, Ohlen DO (1994) Measuring phenological variability from satellite imagery. *Journal of Vegetation Science*, **5**, 703–714.

Richardson AD, Braswell BH, Hollinger DY, Jenkins JP, Ollinger SV (2009) Near-surface remote sensing of spatial and temporal variation in canopy phenology. *Ecological Applications*, **19**, 1417–1428.

Richardson AD, Jenkins JP, Braswell BH, Hollinger DY, Ollinger SV, Smith ML (2007) Use of digital webcam images to track spring green-up in a deciduous broadleaf forest. *Oecologia*, **152**, 323–334.

Schwartz MD (1990) Detecting the onset of spring: a possible application of phenological models. *Climate Research*, **1**, 23–29.

Slaughter DC, Giles DK, Downey D (2008) Autonomous robotic weed control systems: a review. *Computers and Electronics in Agriculture*, **61**, 63–78.

Slayback DA, Pinzon JE, Los SO, Tucker CJ (2003) Northern hemisphere photosynthetic trends 1982–99. *Global Change Biology*, **9**, 1–15.

Soudani K, Le Maire G, Dufrene E, Francois C, Delpierre N, Ulrich E, Cecchini S (2008) Evaluation of the onset of green-up in temperate deciduous broadleaf forests derived from moderate resolution imaging spectroradiometer (MODIS) data. *Remote Sensing of Environment*, **112**, 2643–2655.

Stöckli R, Vidale PL (2004) European plant phenology and climate as seen in a 20-year AVHRR land-surface parameter dataset. *International Journal of Remote Sensing*, **25**, 3303–3330.

Studer S, Stockli R, Appenzeller C, Vidale PL (2007) A comparative study of satellite and ground-based phenology. *International Journal of Biometeorology*, **51**, 405–414.

Thayn JB, Price KP (2008) Julian dates and introduced temporal error in remote sensing vegetation phenology studies. *International Journal of Remote Sensing*, **29**, 6045–6049.

van Vliet AJH, de Groot RS, Bellens Y *et al*. (2003) The European phenology network. *International Journal of Biometeorology*, **47**, 202–212.

Vermote EF, El Saleous N, Justice C (2002) Atmospheric correction of the MODIS data in the visible to middle infrared: first results. *Remote Sensing of Environment*, **83**, 97–111.

Walther G-R, Post E, Convey P *et al*. (2002) Ecological responses to recent climate change. *Nature*, **416**, 389–395.

Wang ZJ, Wang JH, Liu LY, Huang WJ, Zhao CJ, Wang CZ (2004) Prediction of grain protein content in winter wheat (*Triticum aestivum* L.) using plant pigment ratio (PPR). *Field Crops Research*, **90**, 311–321.

Woebbecke DM, Meyer GE, Vonbargen K, Mortensen DA (1995) Color indexes for weed identification under various soil, residue, and lighting conditions. *Transactions of the American Society of Agricultural and Biological Engineers*, **38**, 259–269.

Wolfe DW, Schwartz MD, Lakso AN, Otsuki Y, Pool RM, Shaulis NJ (2005) Climate change and shifts in spring phenology of three horticultural woody perennials in northeastern USA. *International Journal of Biometeorology*, **49**, 303–309.

Zhang X, Friedl MA, Schaaf CF *et al*. (2003) Monitoring vegetation phenology using MODIS. *Remote Sensing of the Environment*, **84**, 471–475.

Zhou LM, Tucker CJ, Kaufmann RK, Slayback D, Shabanov NV, Myneni RB (2001) Variations in northern vegetation activity inferred from satellite data of vegetation index during 1981 to 1999. *Journal of Geophysical Research-Atmospheres*, **106**, 20069–20083.